AIAA SciTech Forum
7-11 January 2019, San Diego, California
AIAA Scitech 2019 Forum

10.2514/6.2019-0152

Spray Cone Formation from Pintle-Type Injector Systems in Liquid Rocket Engines

James Blakely*, Johann Freeberg*, and Jacob Hogge*
University of Southern California, Los Angeles, CA, 90007

Although pintle-type injectors are known for their simplicity and resistance to combustion instabilities, little information regarding their performance is publicly available. Of particular interest is the spray cone angle θ, which forms from the collision of the radial and coaxial propellants in the combustion chamber. This angle affects injector face and chamber wall heat transfer and can inform CFD boundary conditions. Previous studies have related θ to the Total Momentum Ratio, which compares the total momentum of fuel to oxidizer, but this relation fails to account for differences in the number and shape of orifices. To provide a more reliable means of predicting θ, an experiment was conducted to determine a more effective relationship between propellant momenta, θ, and the exit geometries of the pintle tip and annulus. These experiments conducted water-flow tests for fuel and oxidizer flow rates between $0.2\,\mathrm{kg/s}$ and $1.0\,\mathrm{kg/s}$ and for pintle tips with both circular and rectangular orifices with aspect ratios of 1:2, 4:5, and 1:1. The results show that when related to the propellant Local Momentum Ratio, which compares the momenta of propellants at individual collision sites, θ is largely independent of pintle tip orifice geometry. These results provide a simple means of predicting θ and can inform the design of future pintle-type injector systems.

I. Nomenclature

A	=	propellant area
α, β	=	curve fit correction factors
BF	=	pintle tip blockage factor
d_o	=	pintle tip orifice diameter
d_p	=	pintle tip diameter
h	=	rectangular orifice height
LMR	=	propellant local momentum ratio
OF	=	propellant mixture ratio
ρ	=	propellant density
t	=	annulus thickness
θ	=	spay cone angle
TMR	=	propellant total momentum ratio
U	=	propellant velocity
w	=	rectangular orifice width

II. Introduction

Recently, the private space sector has seen enormous growth with the addition of dozens of small launch-vehicle startups to the market [1]. These new players often rely on publicly available data and their own resourcefulness to remain cost-competitive against established launch providers. One of the most critical and costly processes in rocket engine development is the design of the engine's injector system, which introduces and atomizes the propellants into the combustion chamber. Injector design challenges often include thoroughly mixing the propellants prior to combustion and avoiding combustion instabilities [2]. Pintle-type injectors, which use a central post (the pintle) to impinge a radial propellant stream with a coaxial sheet (Fig. 1) offer an elegant solution to these problems by providing strong mixing

*Student, Aerospace and Mechanical Engineering, RRB 101, 854 Downey Way, Los Angeles, CA 90089, Student Member.

while maintaining stable combustion [3]. However, due to the proprietary nature of the aerospace industry, as well as pintle-injector's extensive use in ICBM systems, public information on the topic is limited in detail and scope [3, 4].

While several variations of the pintle injector have been developed, this study focuses only on the fixed-area type which consists of two elements: a pintle tip which deflects a central propellant stream into radial spokes and an annular orifice which injects the second propellant as a coaxial sheet [3]. The two fluids impinge in the combustion chamber as shown in Fig. 1, forming a mixed spray cone of angle θ.

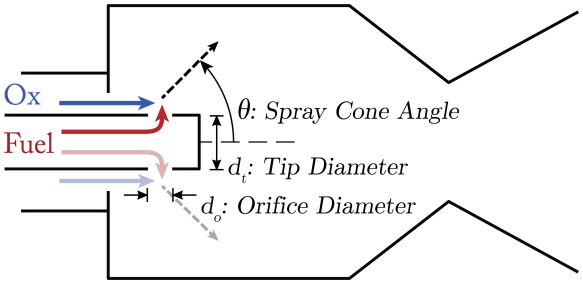

Fig. 1 Pintle injector schematic diagram of operation principles: a central "pintle" deflects radial flow of one propellant into a coaxial stream of the other, forming a mixed spray-cone in the combustion chamber.

Dressler and Bauer highlight how θ affects overall engine performance [5]. The impingement of propellants from a pintle injector produces two distinct recirculation zones in the combustion chamber. The first is the core recirculation zone, which is rich in the radial (central) propellant and shields the pintle tip from combustion temperatures and recirculates the liquid droplets back towards the impingement point for thorough mixing. The second is the mantle recirculation zone, which is rich in the axial (outer) propellant and shields the injector from combustion. The specific geometry of these zones depends on θ.

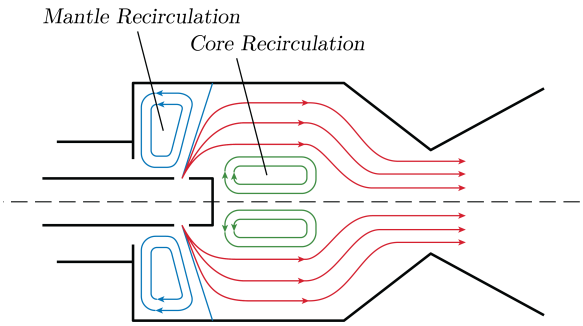

Fig. 2 Expected recirculation zones resulting from impingement of the radial and axial propellants in a combustion chamber (recreated from [5]).

A further application of θ is through the use of propellant film cooling. In this scheme, TMR and BF are selected such that the central propellant penetrates the coaxial sheet and conforms to the chamber wall, providing a mechanism of chamber wall cooling [5]. On the other hand, if propellant adherence to the chamber wall is undesirable, θ can help verify that the combustion chamber is adequately sized. In either case, the basic geometry of the pintle spray affects engine performance and therefore the design process requires a means of predicting θ. Escher ([6]) described θ as a function of both the blockage factor, BF, and the total momentum ratio, TMR, of the two propellants. BF, which represents how much of the pintle tip's circumference is occupied by orifices for radial discharge, is expressed by

$$BF = \frac{N d_o}{\pi d_t}, \tag{1}$$

where d_t is the diameter of the pintle tip, d_o is the diameter or width of each orifice, and N is the number of orifices [3]. From this definition, BF refers to the fraction of axial propellant "blocked" by the radial propellant spokes. BF is illustrated in Fig. 3 and varies between 0 to 1, where $BF = 0$ corresponds to no orifices and $BF = 1$ corresponds to a continuous slot over the entire circumference of the tip.

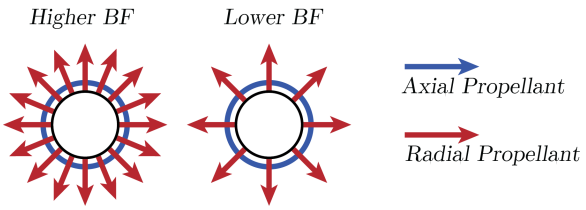

Fig. 3 Illustration of how blockage factor affects pintle tip flow distribution.

TMR is defined as the ratio of the total momentum rate of the radial propellant to the total momentum rate of the axial propellant. This is given by

$$TMR = \frac{(\dot{m}U)_r}{(\dot{m}U)_z}, \tag{2}$$

where U is the propellant velocity and the subscripts r and z denote radial and axial propellant flow, respectively. From conservation of momentum, one might expect θ to follow a kinematic relationship of $\theta = tan^{-1}(TMR)$, but Escher ([6]) found this approach a poor approximation. Alternatively, Escher found that θ scales with $TMR^{1/2}$, as given by Eq. (3):

$$\theta = (105.5 - 24.5TMR)(TMR)^{1/2}. \tag{3}$$

This relation was obtained from water-flow testing for pintle tips with rectangular orifices and blockage factors $BF = 0.3$, 0.6, and 0.8. In addition, these orifices had height:width aspect ratios of 3:1, 1:2, and 7:100, respectively. A reprint of Escher's data is shown in Fig. 4, with Eq. (3) overlaid for comparison.

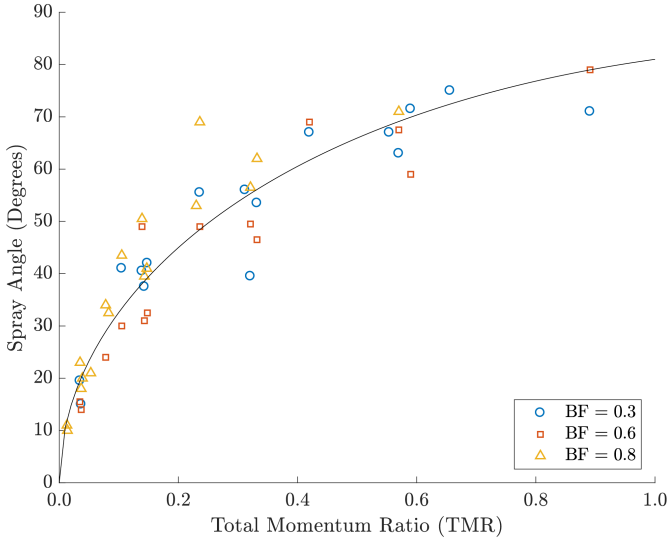

Fig. 4 Experimental relationship between θ and TMR for blockage factors of 0.3, 0.6, and 0.8 (recreated from [6]).

As evidenced from the plot, Eq. (3) describes the general behavior of θ as TMR varies. However, for a given TMR, the difference in θ can be as high as 20°. This is further complicated by differences in BF and orifice aspect ratio between each pintle tip. One explanation for the discrepancy of using TMR to predict θ is that TMR uses aggregate, or three dimensional, flow properties. In reality, the spray cone likely results from propellant collisions at discrete locations and can thus be viewed as a two dimensional phenomenon. To resolve this difference, the local momentum ratio, LMR, is defined by Eq. (4)

$$LMR = \frac{(\dot{m}_\ell U)_r}{(\dot{m}_\ell U)_z} = \frac{(\rho U^2 A_\ell)_r}{(\rho U^2 A_\ell)_z}, \tag{4}$$

where subscript ℓ denotes properties local to individual collision sites rather than across the entire injector. For the radial propellant, A_ℓ refers simply to the area of a single orifice. For the axial propellant, A_ℓ refers only to the area of propellant expected to collide with an individual radial jet. This is illustrated in Fig. 5 below.

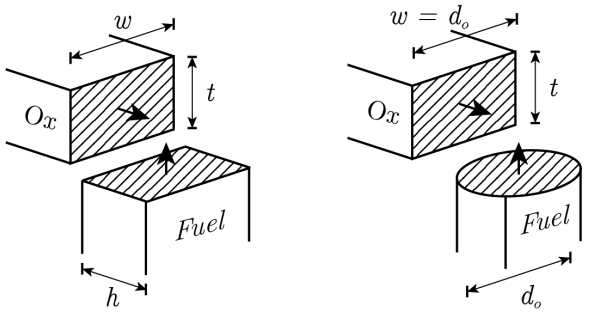

Fig. 5 Diagram of local propellant collision site geometry by pintle-tip orifice shape. Here, t is the thickness of the axial propellant annulus, w and h are the width and height of a rectangular pintle tip orifice, and d is the diameter of a circular pintle tip orifice.

Because Eq. (4) reduces the problem to that of a two dimensional collision, it is expected that the collisional physics approach will become more appropriate when put in terms of LMR. Thus, θ can be predicted from conservation of momentum as

$$\theta = tan^{-1}(LMR). \tag{5}$$

This approach is expected to provide a more consistent means of approximating θ than the use of TMR because it offers a simplification that discounts the quantity of axial propellant not involved in each collision. A similar method is proposed in [7], which treats the collision of two propellant jets from an impinging-stream type injector as a perfectly inelastic collision. However, the lack of available test data makes it difficult to confirm either this approach or the approach taken by Escher. The objective of this research was therefore to design and manufacture a pintle-type injector system to determine a relationship between θ, injector orifice geometry, and propellant momenta. An experiment was conducted to measure θ between a range of 0° and 90° and the corresponding propellant momenta for pintle tips of varying BF and orifice shape. Results were then used to assess the use effectiveness TMR and LMR in predicting θ.

III. Materials and Methods

To collect the necessary data, a pintle-type injector and feed system were designed and manufactured. These components were configured as shown in Fig. 6, which provides an overview of the experimental apparatus. A nitrogen cylinder was used to drive the oxidizer and fuel (simulated with water) from their respective tanks. Variation of the propellant momenta and flow measurement were provided by means of a feed system which supplied the propellants to the injector. Interchangeable pintle tips of different blockage factors and orifice geometries were manufactured and the resulting spray cone was recorded with a DSLR.

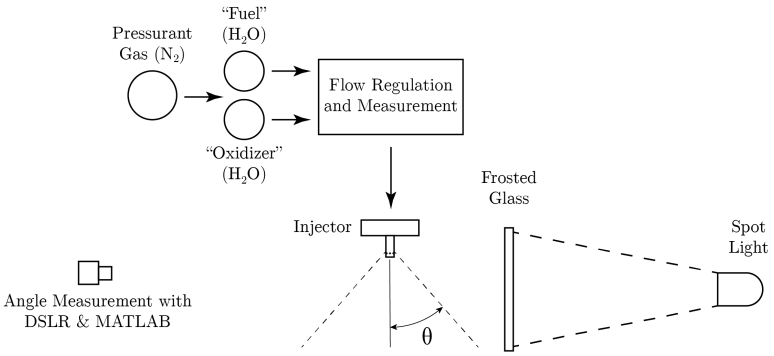

Fig. 6 Top-level diagram of the experimental setup.

The injector and feed system were sized based on the research needs of USC's Rocket Propulsion Laboratory, which sought a bi-propellant, liquid oxygen (LOX) and kerosene engine with 4.5 kN (1000 lbs) of thrust and a chamber pressure of 17 bar (250 psi). Using these parameters and an assumed oxidizer-to-fuel ratio of $OF = 2$, NASA's Chemical Equilibrium Applications (CEA) program was used to generate the expected combustion properties. The program yielded the a required mass flow rate $\dot{m} = 1.8\,\mathrm{kg/s}$ of the two propellants. Assuming $OF = 2$, the nominal operating mass flow rates of the oxidizer and fuel lines were calculated as $\dot{m}_o = 1.2\,\mathrm{kg/s}$ and $\dot{m}_f = 0.6\,\mathrm{kg/s}$, respectively. These values were fed into one-dimensional energy loss calculations to determine the required length and diameter of the supply lines and orifice injector exit areas.

A. Injector Design

The above requirements were used to design the pintle injector shown in Fig. 7.

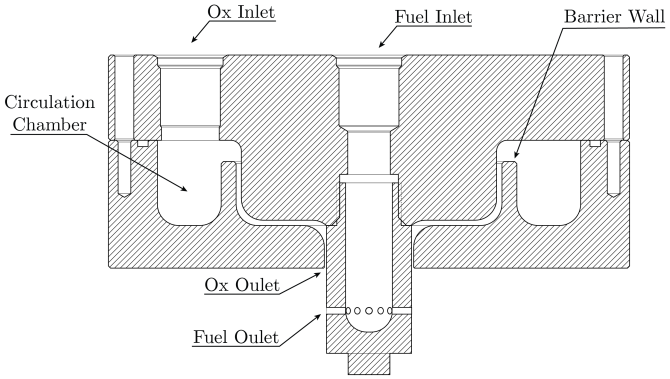

Fig. 7 Cross-sectional view of injector design.

The modular injector body was designed to be geometrically similar to previously studied fixed-area pintle injectors (such as that used by Escher) and to interface with interchangeable threaded tips. For comparability to Escher, the fuel and oxidizer (both simulated with water) were selected as the radial and axial propellants, respectively. Using a target pressure drop of 15 %, one-dimensional pressure loss and exit velocity calculations were used for initial sizing and later verified with Ansys CFX, a commercial CFD software. The design was then iterated to ensure an even mass flow distribution from the annulus (and therefore an even cone angle). To further ensure flow symmetry, concentricity was required and achieved through locating pins. Tight tolerances were achieved by manufacturing all components on a Haas VM-1 CNC Mill reserved for exclusive use, which allowed fabrication of parts to within ±0.0005 in of the design specifications.

Seven pintle tips were designed and manufactured, the details of which are provided in Fig. 10 (see Results). According to Escher's personal correspondence with TRW (now owned by Northrop Grumman), the company advised

the use of pintle tips with $0.3 < BF < 0.7$. For this reason, tips were selected within this range. Similarly, Escher writes that TRW recommended the use of rectangular orifices. To investigate how orifice geometry affects θ, both rectangular and circular orifices were selected. Three of these tips used circular orifices with $BF = 0.35$, $BF = 0.45$, and $BF = 0.55$ while the other four tips used rectangular orifices. For comparison with Escher, a tip of $BF = 0.6$ and aspect ratio of 1:2 was fabricated, but manufacturing constraints prevented exact replication. Three other tips with $BF = 0.55$ and aspect ratios of 1:2, 4:5, and 1:1 were made to study the effect of orifice aspect ratio at a constant BF.

B. Feed System Design

The feed system shown in 8 was designed to allow start-up and shut-off control and to regulate and measure the mass flow of each propellant.

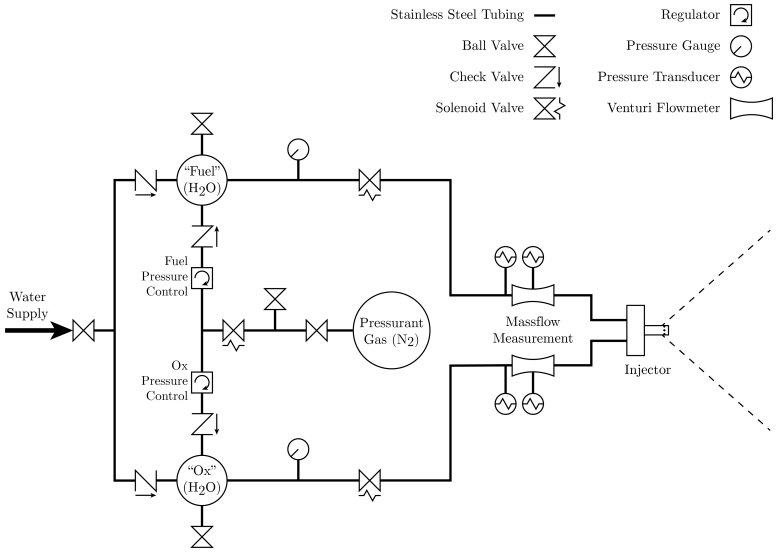

Fig. 8 Schematic diagram of experimental feed system.

As shown, a solenoid valve controlled the flow of the nitrogen pressurant into the propellant tanks. A three-way solenoid was used for this purpose to allow pressure relief in the supply lines after operation. Two additional solenoids were positioned downstream of each tank and were simultaneously actuated by means of a voltage switch. The propellants were driven by the pressure difference between the propellant tank and atmosphere. Pressure regulators positioned upstream of the propellant tanks allowed for independent control of the fuel and oxidizer flow rates, and consequently, the propellant momenta. Check valves were positioned between the tanks and regulators to prevent the back flow of water into the regulators and pressure supply lines. The mass flow $\dot{m}$ of each line was calculated from differential pressure transducer measurements in a calibrated venturi flow meter. Exit velocities from the injector were obtained assuming $\dot{m} = \rho V A$, where A is the relevant exit area. These quantities were used to calculate TMR and LMR from Eq. 2 and 4.

C. Angle Measurement

A MATLAB Digital Image Processing (DIP) script was developed to provide repeatable angle measurements. The DIP technique required high contrast videos of the spray for best results. This was achieved by using a 200 W spot light and frosted glass to create a bright and uniform back-drop behind the injector (Fig. 6).

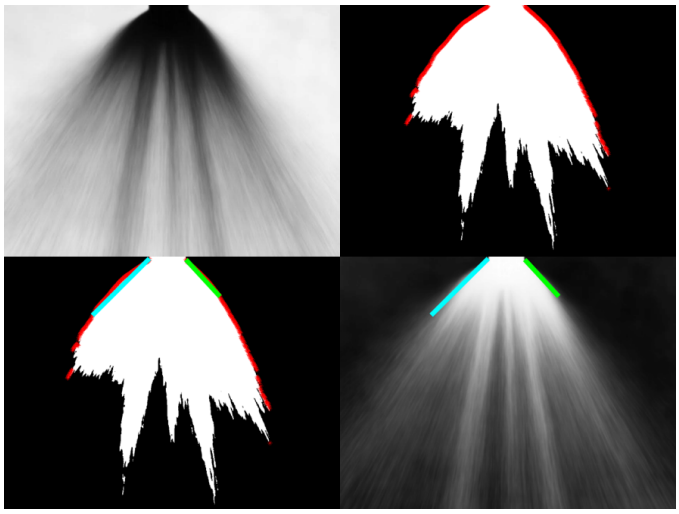

Fig. 9 (Top Left) High-contrast composite image of back-lit spray-cone. (Top Right) Binary mask of thresholded spray-cone. (Bottom Left) Trace and angular measurement from binary mask. (Bottom Left) Angle-lines overlaid on composite image.

Video footage of the spray was shot at 30 frames per second with a resolution of 1920x1080 pixels. The spray video was then imported into MATLAB, converted to gray-scale, and split into its component frames. These frames were then averaged into a composite image of the entire test. This composite image provides information on every path taken by the water during the test, providing a visualization of the aggregate spray pattern. The gray-scale composite image was then color inverted for better visual interpretation. In order to isolate relevant flow from background noise, a threshold was set for one standard deviation above the mean intensity in each composite image and a binary mask was created. The top most portion of this shape was then traced, representing the trajectory of the spray. From this trajectory, a modified linear curve-fit was applied to the left and right sides of each image, starting from the divergence point between the spray and the tip hardware, and ending where the distance between each pixel exceeded the mean distances of all pixels before it. From these curve fits, angles were measured out from the centerline and averaged between the left and right side. Uncertainty was calculated based on the difference between left and right angle measurements. Images from each stage of the DIP method are shown in Fig. 9.

IV. Results

Specific details regarding each tip are provided in Fig. 10 below. Angle measurements were collected by varying the radial ("fuel") mass flow rate between 0.2 kg/s and 0.5 kg/s and by varying the axial ("oxidizer") mass flow rate between 0.3 kg/s and 1 kg/s. These values corresponded to radial velocities between $4 - 10$ m/s and axial velocities between $5 - 20$ m/s.

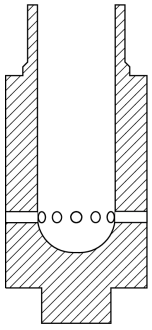

Tip No.	BF	Orifice Shape	No. Orifices	d_o or w [in]	h [in]	h:w	A_o [in²]
1	0.35	○	14	0.0785	-	-	4.84E-03
2	0.45	○	18	0.0785	-	-	4.84E-03
3	0.55	○	22	0.0785	-	-	4.84E-03
4	0.60	▭	30	0.0625	0.0315	0.5	1.97E-03
5	0.55	□	22	0.0785	0.0625	0.8	4.91E-03
6	0.55	▭	22	0.0785	0.0395	0.5	3.10E-03
7	0.55	□	22	0.0785	0.0785	1.0	6.16E-03

Fig. 10 Table specifying defining geometry for each pintle tip.

Angle measurements are plotted against TMR for $0 \leq TMR \leq 4.5$ in Fig. 11. In addition, the inverse tangent

calculated as a function of TMR and Escher's curve fit (Eq. 3) are overlaid for comparison.

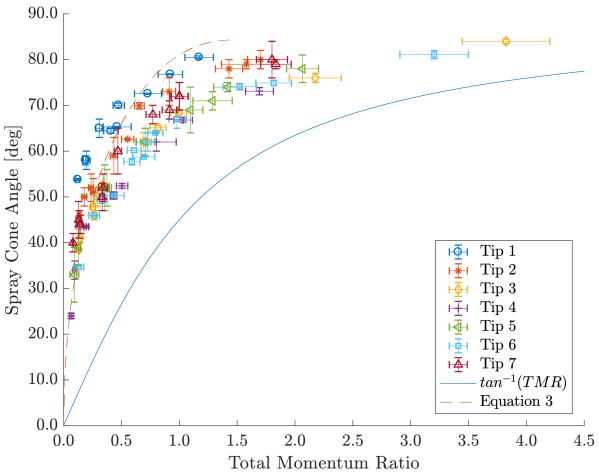

Fig. 11 Spray cone angle θ plotted against the total momentum ratio TMR. The curve fit from [6] and the inverse tangent are plotted for comparison.

The figure shows that the inverse tangent approach poorly approximates the measured data when calculated as a function of TMR. However, Eq. (3) tends to predict θ for $TMR \lessapprox 0.25$ and diverges for $TMR \gtrapprox 0.5$. In particular, Tip 4 ($BF = 0.60$, aspect ratio of 1:2), which was intended to anchor the study's results to Escher's data, was equal to Eq. (3) for $TMR \lessapprox 0.5$ but similarly diverged thereafter. Additionally, the plot shows that Tip 1, which had the lowest BF, had the highest sensitivity to TMR. For the tips with circular orifices, values of θ decreased with increasing BF at the same values TMR. On the other hand, Tips 3 ($BF = 0.45$, circular orifices), 4 ($BF = 0.6$, 1:2 rectangular orifices), and 6 ($BF = 0.6$, 4:5 rectangular orifices) tended to yield equal values of θ for the same TMR while tip 7 ($BF = 0.55$, 1:1 rectangular orifices) tended to provide higher θ.

To compare LMR with TMR, data was plotted in Fig. 12 in terms of LMR and the inverse tangent approximation of Eq. (5) is overlaid. The figure shows that non-dimensionalizing momenta in terms of LMR (as opposed to TMR) causes values of θ to collapse on one another. Additionally, the inverse tangent becomes a stronger approximation for θ, particularly for $LMR \gtrapprox 1$. For $LMR \gtrapprox 0.5$, values of θ tend to fall within 10° for similar LMR regardless of BF, orifice shape, or orifice aspect ratio.

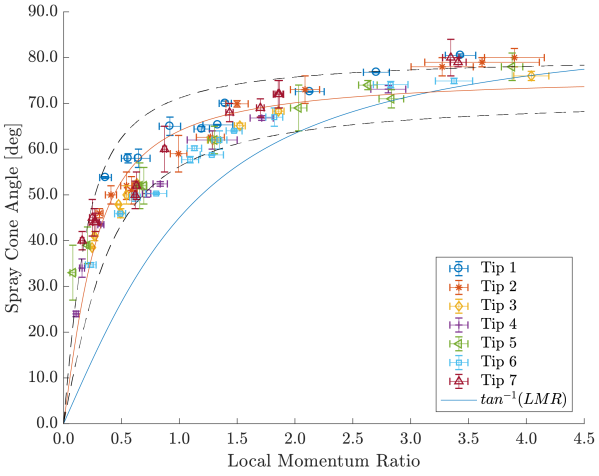

Fig. 12 Spray cone angle θ plotted against the local momentum ratio TMR. Curve fit from [6] and the inverse tangent are plotted for comparison.

To allow for further comparison between pintle tips, the MATLAB "cftool" was used to derive curve fit relations between LMR and θ. These relations assume an inverse tangent function of the form $\theta = \alpha tan^{-1}(\beta LMR)$, where α and β are dimensionless constants. Across tips, α was found to be roughly constant while β varied with no apparent relationship to BF or orifice geometry. For this reason, a single curve fit relation was derived with $\alpha = 0.85 \pm 0.05$ and $\beta = 4 \pm 1$. This is plotted in Fig. 13 below.

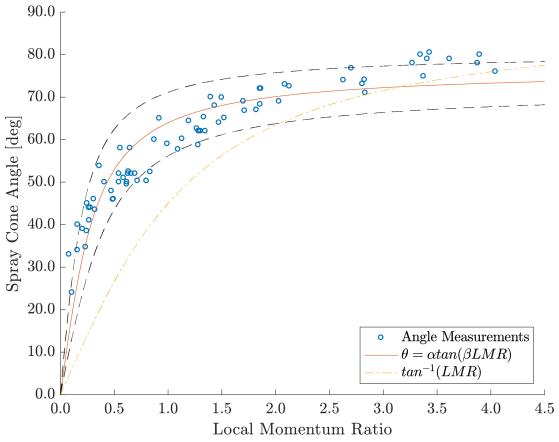

Fig. 13 Averaged curve fit relation of the form $\theta = \alpha tan^{-1}(\beta LMR)$. The upper and lower bounds of the curve fit's uncertainty are also plotted.

As shown, the curve fit relation increases sharply for $LMR \lessapprox 0.5$ before plateauing toward $\theta = 70°$ for $LMR \gtrapprox 1.5$. However, the curve fit loses validity for $LMR \gtrapprox 3.0$. This results from the constraint that at $LMR = 0$, $\theta = 0$. While intuitive, this condition was exceedingly difficult to achieve in practice; values of $\theta \lessapprox 20°$ could not be obtained. A quantity of radial flow seemed to displace the axial flow and create a measurable angle. By pegging the the vertical intercept to 20° with $\alpha = 0.7 \pm 0.05$ and $\beta = 2.0 \pm 0.5$, the overall applicability of this curve fit improves as shown in Fig. 14 below.

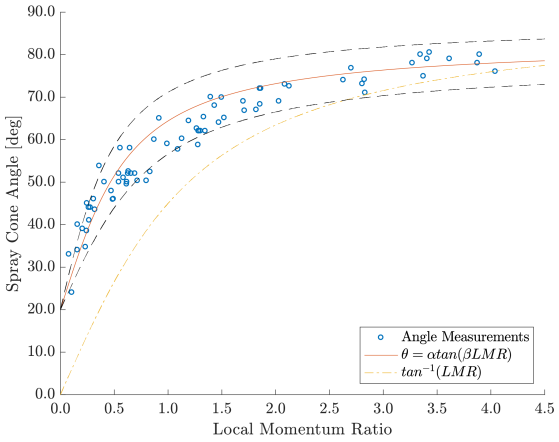

Fig. 14 Improved curve fit relation with 20° offset.

V. Discussion

Figures 11 and 12 demonstrate that the total and local momentum ratios offer differing predictions of θ. However, the LMR approach yields a lower apparent variation between pintle tips, indicating that θ has little dependence on BF,

orifice shape, or aspect ratio. Moreover, the figures show that for each tip at a given θ, the corresponding values of TMR and LMR merely differ by roughly a factor of the tip's blockage factor. Putting the data in terms of LMR normalizes it by removing the blockage factor dependency. This is explained by the fact that if the annulus thickness t is much smaller than the pintle tip diameter d_p, the product $BF \times LMR$ can be simplified to

$$BF \times LMR = \frac{Nw}{\pi d_p} \times \frac{\rho_r U_r^2 wh}{\rho_z U_z^2 wt} = \frac{\rho_r U_r^2 Nwh}{\rho_z U_z^2 \pi d_p t} \approx \frac{\rho_r U_r^2 A_r}{\rho_z U_z^2 A_z} = \frac{(\dot{m}U)_r}{(\dot{m}U)_z} = TMR, \tag{6}$$

where Ar and A_z are the total area of the radial and outer propellants, respectively. When normalized in terms of LMR, the effects of varying orifice shape on collision are not readily detectable by video analysis.

As mentioned, Escher's curve fit (Eq. (3)) was only equal to measured data for low TMR. Given that Escher's measurements often deviated by as much as 20°, this curve was intended only to approximate his data. Tip 5, which was meant to mirror Escher's $BF = 0.6$, did not help resolve differences between the two studies. Furthermore, Escher noted that a term he describes as the "Effective Momentum Ratio," which is defined almost identically to LMR, did not improve his correlations. This is the opposite of what was found in this study which shows that LMR reduces variation between tips.

Figure 12 shows that measurements of θ overshoot the collisional model in all cases. This is particularly true for $LMR \lessapprox 0.5$, where measurements overshoot by as much 30°. An explanation for this is that the collisional model idealizes each collision as two-dimensional and perfectly inelastic. In reality, the pintle tip introduces both collisional and shear mixing between the propellant streams. This shear mixing results in the deflection of propellant upon impact, causing droplets to leave the two-dimensional plane. The fact that the data points overshoot (as opposed to undershoot) indicates that this shear mixing effect is more pronounced for the axial propellant than the radial one. This results in a lower mass flow rate and lower velocity in the denominator of Eq. (4), corresponding to higher θ. Evidence of this was observed during tests, as regions where uninterrupted coaxial spray collided with the ground were clearly visible. The fact that the overshoot effect is more apparent for $LMR \lessapprox 0.5$ may indicate that the mere presence of the radial jets results in some deflection of the axial propellant. As LMR increases, the momentum and energy of the radial propellant increases relative to the axial propellant, resulting in atomization and deflection (shear mixing) of the radial propellant as well. This effect may counterbalance the effect of axial propellant deflections, resulting in θ closer to what the collisional model would predict.

The derived curve fits in Fig. 13 and 14 highlight the difference between measured data and the collisional model. Mathematically, the β term in the curves' argument horizontally compresses the inverse tangent function, an effect expected by apparent reductions in the denominator of Eq. (4). In this light, β represents the amount of energy loss and deflection in the axial propellant. While β causes the expected value of θ to increase, the α term causes it to decrease. The α term therefore accounts for the inelasticity of the collision and energy loss in the radial propellant. As shown, allowing the curve to intercept the vertical axis above zero increases its validity across the collected data. This forces the non-physical condition that for $LMR = 0$, $\theta \neq 0$. As mentioned, $\theta \lessapprox 20°$ could not be achieved in the experiment. Allowing a non-zero intercept accounts for the fact that the fluid streams are of a finite size. In contrast the collisional model neglects fluid volume and approximates their collision as infinitesimal. Overall, these results show that the collisional model can be used to normalize tips of varying BF and provide a rough estimate of θ. However, energy losses and the three-dimensional effects of shear mixing and propellant atomization require the use of the α and β correction factors.

While the above results describe a more robust means of predicting θ, they do not address the question of which test case provides the strongest engine performance. Although this study was not intended to answer that question, several observations can be made. First, a BF between 0.3 and 0.7 allows for adequate shear mixing between the radial and axial streams, while maintaining an axisymmetric flow profile. Second, because this study failed to find measurable differences between tip-geometries, spray-cone angle should not be used as a selection criteria for that particular parameter. While circular orifices have the advantage of manufacturing simplicity, the greater levels of dynamic instability found in rectangular liquid jets ([8]) could lead to greater levels of atomization at the point of impingement, which is desirable for combustion. This, in addition to the fact that rectangular orifice areas can be easily modified by use of a sleeve mechanism, could be the reason that TRW recommended their use [6].

VI. Conclusions

The objective of this research was to investigate the relationships between the spray cone angle, total and local momentum ratios, and pintle-tip geometry. In particular, the study shows that a two-dimensional collisional physics

model can better predict θ than the previously-used total momentum ratio. Moreover, the study shows little measurable difference between pintle-tip blockage factors and aspect ratios, which supports the validity of the collisional physics approach. However, the data shows deviations between measurement and the collisional model which likely result from the three-dimensional effects of propellant shear mixing, energy loss, and atomization. These effects are accounted for by the use of correction factors that together describe the effectiveness of the collision.

Future studies could involve three dimensional imaging of the spray cone to allow for a better understanding of propellant interaction. This might provide a more clear relationship between θ and the curve-fit correction factors. Similarly, varying the overall size of injector geometry (as opposed to only the pintle-tip orifices) could shed further light on the correction factors. Lastly, cold flow testing with actual propellants can be used to determine the role that fluid properties play in the collision and better approximate the actual combustion environment.

Acknowledgements

We would like to thank Dr. Matthew Gilpin for his patience and crucial guidance throughout this research.

References

[1] Bowler, T., "The Disruptors - The new space race," *BBC News*, 2017.

[2] Huzel, D., K, and Huang, D., H, *Modern Engineering for Design of Liquid-Propellant Rocket Engines*, 2nd ed., AIAA, New York, 1992, Chaps. 7, 14.

[3] Heister, S., D, *Handbook of Atomization and Sprays*, 2nd ed., Springer, New York, 2011, Chap. 28.

[4] Rezende, R., N, Pimenta, A., and de Castro Perez, V., "Experiments with Pintle Injector Design and Development," *51st AIAA/SAE/ASEE Joint Propulsion Conference*, AIAA, Orlando, FL, 2015, pp. 1–2.

[5] Dressler, G., A, and Bauer, M., J, "TRW Pintle Engine Heritage and Performance Characteristics," *AIAA*, 2000, pp. 1–22.

[6] Escher, D., W, "Design and Preliminary Hot Fire and Cold Flow Testing of Pintle Injectors," *The Pennsylvania State University Graduate School*, 1996, pp. 1–186.

[7] Sutton, G., P, and Biblarz, O., *Rocket Propulsion Elements*, 8th ed., Wiley and Sons, New Jersey, 2010, Chap. 8.

[8] Tam, C., and Thies, A., "Instability of rectangular jets," *Journal of Fluid Mechanics*, Vol. 248, 1993, pp. 425–448.